https://doi.org/10.5194/essd-2019-79
Preprint. Discussion started: 1 July 2019

Open Access Earth System Science Data Discussions

A Last Glacial Maximum forcing dataset for ocean modelling

Anne L. Morée[1], Jörg Schwinger[2]

[1]Geophysical Institute, University of Bergen and Bjerknes Centre for Climate Research, Bergen, 5007, Norway
[2]NORCE Climate, Bjerknes Centre for Climate Research, 5007 Bergen, Norway

Correspondence to: Anne L. Morée (anne.moree@uib.no)

Abstract. Model simulations of the Last Glacial Maximum (LGM, ~21 000 years before present) can aid the interpretation of proxy records, help to gain an improved mechanistic understanding of the LGM climate system and are valuable for the evaluation of model performance in a different climate state. Ocean-ice only model configurations forced by prescribed atmospheric data (referred to as "forced ocean models") drastically reduce the computational cost of paleoclimate modelling as compared to fully coupled model frameworks. While feedbacks between the atmosphere and ocean-sea-ice compartments of the Earth system are not present in such model configurations, many scientific questions can be addressed with models of this type. The data presented here are derived from fully coupled paleoclimate simulations of the Palaeoclimate Modelling Intercomparison Project (PMIP3). The data are publicly accessible at the NIRD Research Data Archive at https://doi.org/10.11582/2019.00011 (Morée and Schwinger, 2019). They consist of 2-D anomaly forcing fields suitable for use in ocean models that employ a bulk forcing approach. The data include specific humidity, downwelling longwave and shortwave radiation, precipitation, wind (v and u components), temperature and sea surface salinity (SSS). All fields are provided as climatological mean anomalies between LGM and pre-industrial times. These anomaly data can therefore be added to any pre-industrial ocean forcing data set in order to obtain forcing fields representative of LGM conditions as simulated by PMIP3 models. These forcing data provide a means to simulate the LGM in a computationally efficient way, while still taking advantage of the complexity of fully coupled model set-ups. Furthermore, the dataset can be easily updated to reflect results from upcoming and future paleo model intercomparison activities.

1 Introduction

The LGM (~21 kya) is of interest to the climate research community because of the relative abundance of proxy data, and because it is the most recent profoundly different climatic state of our planet. For these reasons, the LGM is extensively studied in modelling frameworks (Menviel et al., 2017; Brady et al., 2012; Otto-Bliesner et al., 2007). Model simulations of the past ocean can not only provide a method to gain a mechanistic understanding of marine proxy records, they can also inform us about model performance in a different climatic state of the Earth system (Braconnot et al., 2012). Typical state-of-the-art tools to simulate the (past) Earth system are climate or Earth system models as, for example, used in the Climate Model Intercomparison Project phase 5 (CMIP5; Taylor et al. (2011)). Unfortunately, the computational costs and run-time of such fully coupled model frameworks are a major obstacle for their application to palaeoclimate modelling. Palaeoclimate modelling optimally requires long (thousands to ten thousands of years) simulations in order to provide the necessary time for relevant processes to

https://doi.org/10.5194/essd-2019-79
Preprint. Discussion started: 1 July 2019

Open Access Earth System Science Data Discussions

emerge (e.g. CaCO3 compensation) (Braconnot et al., 2007). Complex CMIP-type fully coupled models can typically not be run into full equilibrium (which requires hundreds to thousands of years of integration) due to computational costs (Eyring et al., 2016). Therefore, these models exhibit model drift (especially in the deep ocean, e.g. Marzocchi and Jansen (2017)). The 3rd phase of the PMIP project (PMIP3; Braconnot et al. (2012)) limits global mean sea-surface temperature drift to under 0.05 K per century and requires the Atlantic Meridional Overturning Circulation to be stable (Kageyama et al., 2018).

The use of PMIP output as ocean forcing is an accepted practice in ocean modelling (e.g., Muglia and Schmittner (2015)). We refer to a "forced ocean model" as a model of the ocean-sea-ice-atmosphere system in which the atmosphere is represented by prescribed 2-D forcing fields. It can be used whenever ocean-atmosphere feedbacks are of minor importance and has the advantage of reducing the computational costs – making longer or more model runs feasible. We present 2-D (surface) anomaly fields (LGM minus pre-industrial) calculated from monthly climatological PMIP3 output. The PMIP3 output is the result of global boundary conditions and forcings (such as insolation and ice sheet cover) applied in the fully coupled PMIP3 models (Braconnot et al., 2012). Our dataset (Morée and Schwinger, 2019) is a unique compilation of existing data, processed and reformatted such that it can be readily applied in a forced ocean model framework that uses a bulk forcing approach similar to Large and Yeager (2004). Since this approach has been popularized through coordinated model intercomparison activities (Griffies et al., 2009), a majority of forced ocean models today uses this approach. The 2-D anomaly fields presented here can be added to the pre-industrial forcing of a forced ocean model in order to obtain an atmospheric forcing representative of the LGM. The data are climatological mean anomalies, and as such suitable for equilibrium LGM 'time-slice' modelling of the ocean. The description of the procedure followed to make this dataset (Sect. 3, Table 3) should support any extension of the dataset with additional (PMIP-derived) variables if needed. The PMIP4 guidelines (Kageyama et al., 2017) can support users in designing a specific model set-up, for example regarding the land-sea mask, trace gas concentrations, river outflow or other conditions and forcing one would want to apply to a model. In Sect. 2, a general description of the dataset and data sources is provided alongside with an overview of the variables (Table 1).

2 General description of the dataset

The data presented in this article are 2-D anomaly fields of the LGM versus pre-industrial state (LGM minus pre-industrial) based on the PMIP3 (Braconnot et al., 2012). These anomaly fields can be used as atmospheric LGM forcing fields for ocean-only model set-ups when added to pre-industrial forcing fields. The basis of this data is monthly climatological PMIP3 output. Any variables presented on sub-monthly time resolution are therefore time-interpolated. Since this is a limitation of the available data, we have to assume that any sub-monthly variability (e.g. the diurnal cycle) is preserved from the preindustrial climate state to the LGM state. The anomalies are calculated as the mean of the difference between monthly climatologies of the 'lgm' and 'piControl' PMIP3 model runs (denoted LGM and PI hereafter). In cases where modelling groups provided more than one ensemble member, we included only the first member in our calculations. Even though PMIP3 simulations have limitations and a large inter-model spread, PMIP3 is the state of the art for modelling of past climates at present (Braconnot et al., 2012; Braconnot and Kageyama, 2015). Furthermore, no global proxy-based reconstructions of the variables presented here are available to provide a proxy-based LGM forcing dataset. Using mean coupled model output as

https://doi.org/10.5194/essd-2019-79
Preprint. Discussion started: 1 July 2019

forcing is thus considered the best available option for use in forced ocean models. The data is the mean anomaly of four PMIP3 models (CNRM-CM5, IPSL-CM5A-LR, MIROC-ESM and MRI-CGCM3, Table 2), as only these models provide output for all variables.

The variables are i) specific humidity at 10 meters, ii) downwelling longwave radiation, iii) downwelling shortwave radiation, iv) precipitation, v) wind (v and u components), vi) temperature at 10 meters, and vii) sea surface salinity (SSS) (Table 1). The SSS anomaly field can be used to apply SSS restoring in LGM simulations.

All variables (Sect. 3.1-7) of the monthly climatological PMIP3 output have been regridded (Table 3, #1), averaged (Table 3, #2), and differenced (Table 3, #3) to calculate the anomaly fields. Changes in the order of the operations leads to differences in the order of round-off errors only. Additional procedures for each variable is given in the respective part of Sect. 3, together with a figure of each variable's yearly mean anomaly and model spread. All operations were performed with either CDO version 1.7.0 (Schulzweida, 2019) or NCO version 4.6.9. Main functions used are documented in Table 3 and referred to in the text at the first occurrence. The atmospheric anomaly data are on a Gaussian grid, with 192×94 (lon×lat) grid-points. The SSS fields is on a regular 360×180 (lon×lat) grid. Regridding any of the files to a different model grid should be straightforward (e.g., Table 3, #1), as it was ensured that all files contain the information needed for re-gridding. The variables, grid and time resolution are chosen to be compatible with the CORE forcing fields (Large and Yeager, 2004), which have been extensively used in the ocean modelling community (e.g. Griffies et al. (2009); Schwinger et al. (2016)). We anticipate that the variables selected here should be useful in different model set-ups as well. In the case of NorESM-OC (Schwinger et al., 2016), the atmospheric anomaly fields were added to its CORE normal-year forcing fields (Large and Yeager, 2004) to obtain a LGM normal-year forcing. Note that the addition of the anomaly fields to the user's own model forcing could lead to physically unrealistic/not-meaningful results for some variables (such as negative precipitation or radiation). This must be corrected for by capping off sub-zero values (Table 3, #4) after addition of the anomaly.

3 The variables

3.1 Specific humidity anomaly

The monthly climatology of near-surface specific humidity is provided at 2 meters height in PMIP3. The bulk forcing method of Large and Yeager (2004) requires specific humidity (and temperature) at the same height as the wind forcing (10 meters). Therefore, specific humidity was re-referenced to 10 meters height for each of the four models following the procedure detailed in Large and Yeager (2004). The re-referencing required the use of wind (u and v components), sea level pressure and skin temperature (sea surface temperature over the open ocean), which were taken from the respective PI and LGM PMIP3 output for each model. The mean anomaly over the four models was time interpolated (Table 3, #5) to a 6-hour time resolution from the monthly climatological PMIP3 output. The annual mean LGM-PI anomaly field (Fig. 1) shows a global decrease in specific humidity, as expected from decreased air temperatures (Sect. 3.6). The anomaly is most pronounced around the equator, where we see a decrease of 2-3 kg kg^{-1}, while the anomaly is near-zero towards both poles. The model spread of the anomaly shows a disagreement between the PMIP3 models generally in the order of 1-2 kg kg^{-1}, without any strong spatial pattern (Fig. 1).

https://doi.org/10.5194/essd-2019-79
Preprint. Discussion started: 1 July 2019

Open Access Earth System Science Data Discussions

3.2 Downwelling longwave radiation anomaly

The anomaly for surface downwelling longwave radiation is time-interpolated (Table 3, #5) to a daily time resolution. The annual mean anomaly field (Fig. 2) shows globally decreased downwelling longwave radiation in the LGM as compared to the PI, in the order of 10-30 W m^{-2} over most of the ocean due to a generally cooler atmosphere (Sect. 3.6). The largest anomalies lie at the northern ice sheets, with up to -146 W m^{-2} lower radiation in the LGM than in the PI. In addition to influencing radiative forcing over land, ice is likely also the main contributor to the high (60-90 W m^{-2}) inter-model spread in North Atlantic. The remainder of the ocean exhibits a better agreement, with inter-model spreads generally below 20 W m^{-2} (Fig. 2).

3.3 Downwelling shortwave radiation anomaly

The surface downwelling shortwave radiation anomaly field is time-interpolated (Table 3, #5) to daily fields as done for downwelling longwave radiation. The annual mean anomaly is especially pronounced around the Laurentide and Scandinavian ice sheets, where strong positive anomalies of over ~30 W m^{-2} exist (Fig. 3). Globally, the annual mean downwelling shortwave radiation anomaly generally falls in a range of -15 to +15 W m^{-2} over the ocean. The anomaly field shows negative anomalies as well positive ones in an alternating spatial pattern approximately symmetrically around the equator in the Pacific basin. The inter-model spread is largest in the North Atlantic region and along the equator (Fig. 3). Due to the large model disagreement of up to 50 W m^{-2} for this variable, the inter-model spread and mean anomaly are of similar magnitude although a consistent pattern is present in the anomaly field.

3.4 Precipitation anomaly

The anomaly presented here is the LGM-PI precipitation anomaly at the air-sea interface and includes both the liquid and solid phases from all types of clouds (both large-scale and convective). The units were converted to mm day^{-1}. The resulting annual mean anomaly generally falls in the range of -2 to 2 mm day^{-1}, and is most pronounced along the equator and in the Northern Hemisphere (Fig. 4). The models show a mean increase in precipitation directly south of the equator in the Pacific basin, as well as in the Pacific subtropics off the western North-American coast. The North Atlantic also receives a mean positive precipitation anomaly, offsetting part of the positive salinity anomaly there, which is potentially relevant for the simulation of deep water formation in this region (Sect. 3.7). Negative mean precipitation anomalies are most pronounced directly north of the equator and north of ~40° N in the Pacific basin as well as in the Atlantic Arctic. The inter-model spread is up to ~5 mm day^{-1} around the equator, likely due to the model disagreement about the sign and location of changes in the inter-tropical convergence zone (Fig. 4).

3.5 Wind anomalies, u and v components

Both for the u and v component of the wind speed, the LGM-PI anomaly is time-interpolated to 6-hourly fields. The annual mean meridional wind velocity (v, southerly winds) anomaly shows a pronounced increase (~3-5 m s^{-1}) in southerly winds around the NW edge of the Laurentide ice sheet as well as over the NW edge of the Scandinavia ice sheet (Fig. 5). Alongside that, a pronounced decrease (~ 3-5 m s^{-1}) in southerly winds is simulated above the Laurentide ice sheet and east of Scandinavia. The open ocean anomalies are generally small (at most ±1

https://doi.org/10.5194/essd-2019-79
Preprint. Discussion started: 1 July 2019

m s^{-1}). The inter-model spread has no pronounced pattern but is sizable, with ~ 1-5 m s^{-1} disagreement between the PMIP3 models. The mean zonal wind velocity (u, westerly winds) anomaly shows alternating negative and positive anomaly bands with an approximate ±2 m s^{-1} range (Fig. 6). This pattern is stronger in the Northern Hemisphere north of ~45° N, where ~5 m s^{-1} anomalies exist over the American continent and the North Atlantic ocean basin. The inter-model spread (~1-3 m s^{-1}) has little structure except for the ~4-5 m s^{-1} disagreement in the Southern Ocean south of ~40° S (Fig. 6).

3.6 Temperature anomaly

The near-surface atmospheric temperature at 2 m height from PMIP3 is re-referenced to 10 meters (as done for specific humidity, Sect. 3.1), and time-interpolated to calculate the 6-hourly mean anomaly for temperature. In order to account for differences in temperature to changes in topography in each of the models, a correction is made for the adiabatic lapse rate. The temperature effect in topography above 10 m is calculated per model using an adiabatic lapse rate effect of 5 degrees per kilometre. The dataset presented here is thus representative of the fictitious temperature at 10 meter above sea level, and should be corrected for the adiabatic lapse rate if applied at a different height (i.e. on land). For flexibility of use, both the topography uncorrected ('tas') and topography corrected ('tas_10m') temperature anomaly data are provided in the netCDF file. The topography-corrected annual mean temperature anomaly is generally negative (~ -3 K), but has extremes around the North Atlantic of around -15 K (Fig. 7). There is a clear pattern in the model spread: The models show a large spread (>10 K) over the continents north of ~45° N, as well as south of ~40° S. At lower latitudes and over the ocean the model spread is generally smaller (0-3 K), with the only exceptions in the Southern Ocean (5-10 K) and in the North Atlantic (>10 K) (Fig. 7).

3.7 Sea surface salinity anomaly

Global mean salinity is initialized in PMIP3 models with a 1 psu higher salinity to account for the concentrating effect of the decrease in sea level (Kageyama et al., 2017). Sea surface salinity however, shows a more variable annual mean LGM-PI change due to changes in the global hydrological cycle (Fig. 8). Only the models CNRM-CM5 and MIROC-ESM are used here for the averaging because of data availability. The difference in land-sea mask between the LGM and PI simulations is accounted for by filling any missing values with a distance-weighted mean based on the four nearest neighbours per empty grid cell (Table 3, #6). This results in a SSS anomaly field with values in every grid cell (so essentially without a land-sea mask), such that it can be used with any land-sea mask. In addition, the sea surface salinity anomaly is presented on a regular 1x1 grid for ease of use. The land-sea mask correction is only needed for SSS, as all other variables presented in this text are global atmospheric fields. Because the mean anomaly is locally patchy due to the large model spread and extrapolation, we improve the smoothness of the result using 9-point smoothing as a final step (Table 3, #7). The resulting annual mean SSS anomaly (Fig. 8) shows an increase in sea surface salinity (~1 psu) over the Southern Ocean south of ~55° S, as well as in the Arctic (>3 psu) and the Northern Indian Ocean (~1 psu). A ~2 psu anomaly is simulated in the Canadian Archipelago, the Labrador Sea and across the North Atlantic between what is now Canada and Europe (Fig. 8). Freshening is simulated close to some continents, and is especially pronounced around Scandinavia (about -3 psu). Simulated ocean circulation can be very sensitive to fresh water forcing and thus SSS, especially in the North Atlantic (e.g. Rahmstorf (1996), Spence et al. (2008)). Application of SSS restoring using the SSS anomaly

https://doi.org/10.5194/essd-2019-79
Preprint. Discussion started: 1 July 2019

field should therefore be done with caution and attention to its effects on the meridional overturning circulation. Tuning of the salinity anomaly in important deep-water formation regions of up to about ±1 psu, such as done by for example Winguth et al. (1999), may be required to obtain a satisfactory circulation field in reasonable agreement with proxy data. Such adjustments fall well within the PMIP3 model spread (Fig. 8), and show the current limitations of fully coupled PMIP3 models to simulate the LGM hydrological cycle consistent with proxy records of ocean circulation.

4 Data availability

The data are publicly accessible at the NIRD Research Data Archive at https://doi.org/10.11582/2019.00011 (Morée and Schwinger, 2019).

5 Summary and Conclusions

The output of the fully coupled PMIP3 simulations of CNRM-CM5, IPSL-CM5A-LR, MIROC-ESM and MRI-CGCM3 is converted to anomaly datasets intended for use in forced ocean modelling of the LGM. All anomalies are calculated as the difference between the LGM and PI PMIP3 experiments. In addition, all data are formatted in a way that further conversions (of for example units or the grid) can be applied in a straightforward way. The variables are provided in netCDF format in separate files, and distributed by the NIRD Research Data Archive (Morée and Schwinger, 2019). A climatological LGM forcing data set can be created for any forced ocean model by addition of the presented 2-D anomaly fields to the model's pre-industrial forcing. This approach enables the scientific community to simulate the LGM ocean state in a forced model set-up. We expect that if additional forcing is needed for a specific model, the same approach as described above can be followed. This process is simplified by providing all main CDO and NCO commands used in creating the dataset (Table 3). All data represent a climatological year, i.e. one annual cycle per variable. The application of the data is thus suitable for 'time-slice' equilibrium simulations of the LGM.

The uncertainty of our anomaly forcing (approximated by the model spread of the PMIP3 models) is generally of similar magnitude as the multi-model annual mean. The attribution of the model spread to specific processes is beyond the scope of this article, but our results show that there is considerable uncertainty involved in the magnitude of the anomaly for all variables presented here. Nevertheless, all mean anomalies show a distinct spatial pattern that we expect to be indicative of the LGM-PI changes. Finally, there is no other way to reconstruct most of these variables than model simulations with state-of-the-art models such as those applied in the PMIP3 experiments. For modelling purposes, the inter-model disagreement of PMIP3 provides the user with leeway to adjust the amplitude of the forcing (guided by the size of the model spread). Such adjustments can improve model-proxy data agreements, such as described for salinity in Sect. 3.7.

Author contributions. AM prepared, visualized and analysed the data and wrote the original draft of the manuscript. AM and JS together conceptualized the method and revised the manuscript. JS provided supervision throughout the study.

Competing interests. The authors declare that they have no conflict of interest.

https://doi.org/10.5194/essd-2019-79
Preprint. Discussion started: 1 July 2019

Acknowledgements. We acknowledge the World Climate Research Programme's Working Group on Coupled Modelling, which is responsible for CMIP, and we thank the climate modelling groups (Table 2) for producing and making available their model output. For CMIP the U.S. Department of Energy's Program for Climate Model Diagnosis and Intercomparison provides coordinating support and led development of software infrastructure in partnership with the Global Organization for Earth System Science Portals. This is a contribution to the Bjerknes Centre for Climate Research (Bergen, Norway). Storage resources were provided by UNINETT Sigma2 - the National Infrastructure for High Performance Computing and Data Storage in Norway (project number ns2980k). Anne L. Morée is grateful for PhD funding through the Faculty for Mathematics and Natural Sciences of the University of Bergen. Jörg Schwinger acknowledges funding through the Research Council of Norway (project INES (270061)). This study is a contribution to the project "Coordinated Research in Earth Systems and Climate: Experiments, kNowledge, Dissemination and Outreach" (CRESCENDO; EU Horizon2020 Programme grant no. 641816) which is funded by the European Commission.

References

Braconnot, P., Otto-Bliesner, B., Harrison, S., Joussaume, S., Peterchmitt, J. Y., Abe-Ouchi, A., Crucifix, M., Driesschaert, E., Fichefet, T., Hewitt, C. D., Kageyama, M., Kitoh, A., Laîné, A., Loutre, M. F., Marti, O., Merkel, U., Ramstein, G., Valdes, P., Weber, S. L., Yu, Y., and Zhao, Y.: Results of PMIP2 coupled simulations of the Mid-Holocene and Last Glacial Maximum; Part 1: experiments and large-scale features, Clim. Past, 3, 261-277, 10.5194/cp-3-261-2007, 2007.

Braconnot, P., Harrison, S., Kageyama, M., Bartlein, P., Masson-Delmotte, V., Abe-Ouchi, A., Otto-Bliesner, B., and Zhao, Y.: Evaluation of climate models using palaeoclimatic data, Nature Climate Change, 2, 417-424, doi: 10.1038/nclimate1456, 2012.

Braconnot, P., and Kageyama, M.: Shortwave forcing and feedbacks in Last Glacial Maximum and Mid-Holocene PMIP3 simulations, Philosophical Transactions of the Royal Society A: Mathematical, Physical and Engineering Sciences, 373, 20140424, 10.1098/rsta.2014.0424, 2015.

Brady, E. C., Otto-Bliesner, B. L., Kay, J. E., and Rosenbloom, N.: Sensitivity to Glacial Forcing in the CCSM4, Journal of Climate, 26, 1901-1925, 10.1175/JCLI-D-11-00416.1, 2012.

Dufresne, J. L., Foujols, M. A., Denvil, S., Caubel, A., Marti, O., Aumont, O., Balkanski, Y., Bekki, S., Bellenger, H., Benshila, R., Bony, S., Bopp, L., Braconnot, P., Brockmann, P., Cadule, P., Cheruy, F., Codron, F., Cozic, A., Cugnet, D., de Noblet, N., Duvel, J. P., Ethé, C., Fairhead, L., Fichefet, T., Flavoni, S., Friedlingstein, P., Grandpeix, J. Y., Guez, L., Guilyardi, E., Hauglustaine, D., Hourdin, F., Idelkadi, A., Ghattas, J., Joussaume, S., Kageyama, M., Krinner, G., Labetoulle, S., Lahellec, A., Lefebvre, M. P., Lefevre, F., Levy, C., Li, Z. X., Lloyd, J., Lott, F., Madec, G., Mancip, M., Marchand, M., Masson, S., Meurdesoif, Y., Mignot, J., Musat, I., Parouty, S., Polcher, J., Rio, C., Schulz, M., Swingedouw, D., Szopa, S., Talandier, C., Terray, P., Viovy, N., and Vuichard, N.: Climate change projections using the IPSL-CM5 Earth System Model: from CMIP3 to CMIP5, Clim Dyn, 40, 2123-2165, 10.1007/s00382-012-1636-1, 2013.

Eyring, V., Bony, S., Meehl, G. A., Senior, C. A., Stevens, B., Stouffer, R. J., and Taylor, K. E.: Overview of the Coupled Model Intercomparison Project Phase 6 (CMIP6) experimental design and organization, Geosci. Model Dev., 9, 1937-1958, 10.5194/gmd-9-1937-2016, 2016.

Griffies, S. M., Biastoch, A., Böning, C., Bryan, F., Danabasoglu, G., Chassignet, E. P., England, M. H., Gerdes, R., Haak, H., Hallberg, R. W., Hazeleger, W., Jungclaus, J., Large, W. G., Madec, G., Pirani, A., Samuels, B. L., Scheinert, M., Gupta, A. S., Severijns, C. A., Simmons, H. L., Treguier, A. M., Winton, M., Yeager, S., and Yin, J.: Coordinated Ocean-ice Reference Experiments (COREs), Ocean Modelling, 26, 1-46, https://doi.org/10.1016/j.ocemod.2008.08.007, 2009.

Kageyama, M., Albani, S., Braconnot, P., Harrison, S. P., Hopcroft, P. O., Ivanovic, R. F., Lambert, F., Marti, O., Peltier, W. R., Peterschmitt, J. Y., Roche, D. M., Tarasov, L., Zhang, X., Brady, E. C., Haywood, A. M., LeGrande, A. N., Lunt, D. J., Mahowald, N. M., Mikolajewicz, U., Nisancioglu, K. H., Otto-Bliesner, B. L., Renssen, H., Tomas, R. A., Zhang, Q., Abe-Ouchi, A., Bartlein, P. J., Cao, J., Li, Q., Lohmann, G., Ohgaito, R., Shi, X., Volodin, E., Yoshida, K., Zhang, X., and Zheng, W.: The PMIP4 contribution to CMIP6 – Part 4: Scientific objectives and experimental design of the PMIP4-CMIP6 Last Glacial Maximum experiments and PMIP4 sensitivity experiments, Geosci. Model Dev., 10, 4035-4055, 10.5194/gmd-10-4035-2017, 2017.

https://doi.org/10.5194/essd-2019-79
Preprint. Discussion started: 1 July 2019

Kageyama, M., Braconnot, P., Harrison, S. P., Haywood, A. M., Jungclaus, J. H., Otto-Bliesner, B. L., Peterschmitt, J. Y., Abe-Ouchi, A., Albani, S., Bartlein, P. J., Brierley, C., Crucifix, M., Dolan, A., Fernandez-Donado, L., Fischer, H., Hopcroft, P. O., Ivanovic, R. F., Lambert, F., Lunt, D. J., Mahowald, N. M., Peltier, W. R., Phipps, S. J., Roche, D. M., Schmidt, G. A., Tarasov, L., Valdes, P. J., Zhang, Q., and Zhou, T.: The PMIP4 contribution to CMIP6 – Part 1: Overview and over-arching analysis plan, Geosci. Model Dev., 11, 1033-1057, 10.5194/gmd-11-1033-2018, 2018.

Large, W. G., and Yeager, S. G.: Diurnal to decadal global forcing for ocean and sea-ice models: the data sets and flux climatologies, Tech. Note NCAR/TN-460+STR. National Center of Atmospheric Research, Boulder, Colorado, USA, 2004.

Marzocchi, A., and Jansen, M. F.: Connecting Antarctic sea ice to deep-ocean circulation in modern and glacial climate simulations, Geophysical Research Letters, 44, 6286-6295, 10.1002/2017GL073936, 2017.

Menviel, L., Yu, J., Joos, F., Mouchet, A., Meissner, K. J., and England, M. H.: Poorly ventilated deep ocean at the Last Glacial Maximum inferred from carbon isotopes: A data-model comparison study, Paleoceanography, 32, 2-17, 10.1002/2016pa003024, 2017.

Morée, A., Schwinger, J.: Last Glacial Maximum minus pre-industrial anomaly fields for use in forced ocean modelling, based on PMIP3, Norstore, https://doi.org/10.11582/2019.00011, 2019.

Muglia, J., and Schmittner, A.: Glacial Atlantic overturning increased by wind stress in climate models, Geophysical Research Letters, 42, 9862-9868, doi:10.1002/2015gl064583, 2015.

Otto-Bliesner, B. L., Hewitt, C. D., Marchitto, T. M., Brady, E., Abe-Ouchi, A., Crucifix, M., Murakami, S., and Weber, S. L.: Last Glacial Maximum ocean thermohaline circulation: PMIP2 model intercomparisons and data constraints, Geophysical Research Letters, 34, 10.1029/2007GL029475, 2007.

Rahmstorf, S.: On the freshwater forcing and transport of the Atlantic thermohaline circulation, Clim Dyn, 12, 799-811, 10.1007/s003820050144, 1996.

Schulzweida, U.: CDO User Guide (Version 1.9.6), Max Planck Institute for Meteorology, Bundesstraße 53, 20146 Hamburg, Germany, http://doi.org/10.5281/zenodo.2558193, 215 pp., 2019.

Schwinger, J., Goris, N., Tjiputra, J. F., Kriest, I., Bentsen, M., Bethke, I., Ilicak, M., Assmann, K. M., and Heinze, C.: Evaluation of NorESM-OC (versions 1 and 1.2), the ocean carbon-cycle stand-alone configuration of the Norwegian Earth System Model (NorESM1), Geosci. Model Dev., 9, 2589-2622, 10.5194/gmd-9-2589-2016, 2016.

Spence, J. P., Eby, M., and Weaver, A. J.: The Sensitivity of the Atlantic Meridional Overturning Circulation to Freshwater Forcing at Eddy-Permitting Resolutions, Journal of Climate, 21, 2697-2710, 10.1175/2007JCLI2103.1, 2008.

Sueyoshi, T., Ohgaito, R., Yamamoto, A., Chikamoto, M. O., Hajima, T., Okajima, H., Yoshimori, M., Abe, M., O'Ishi, R., Saito, F., Watanabe, S., Kawamiya, M., and Abe-Ouchi, A.: Set-up of the PMIP3 paleoclimate experiments conducted using an Earth system model, MIROC-ESM, Geosci. Model Dev., 6, 819-836, 10.5194/gmd-6-819-2013, 2013.

Taylor, K. E., Stouffer, R. J., and Meehl, G. A.: An Overview of CMIP5 and the Experiment Design, Bulletin of the American Meteorological Society, 93, 485-498, 10.1175/BAMS-D-11-00094.1, 2011.

Voldoire, A., Sanchez-Gomez, E., Salas y Mélia, D., Decharme, B., Cassou, C., Sénési, S., Valcke, S., Beau, I., Alias, A., Chevallier, M., Déqué, M., Deshayes, J., Douville, H., Fernandez, E., Madec, G., Maisonnave, E., Moine, M. P., Planton, S., Saint-Martin, D., Szopa, S., Tyteca, S., Alkama, R., Belamari, S., Braun, A., Coquart, L., and Chauvin, F.: The CNRM-CM5.1 global climate model: description and basic evaluation, Clim Dyn, 40, 2091-2121, 10.1007/s00382-011-1259-y, 2013.

Winguth, A. M. E., Archer, D., Duplessy, J. C., Maier-Reimer, E., and Mikolajewicz, U.: Sensitivity of paleonutrient tracer distributions and deep-sea circulation to glacial boundary conditions, Paleoceanography, 14, 304-323, 10.1029/1999PA900002, 1999.

Yukimoto, S., Adachi, Y., Hosaka, M., Sakami, T., Yoshimura, H., Hirabara, M., Tanaka, T. Y., Shindo, E., Tsujino, H., Deushi, M., Mizuta, R., Yabu, S., Obata, A., Nakano, H., Koshiro, T., Ose, T., and Kitoh, A.: A New Global Climate Model of the Meteorological Research Institute: MRI-CGCM3;Model Description and Basic Performance, Journal of the Meteorological Society of Japan. Ser. II, 90A, 23-64, 10.2151/jmsj.2012-A02, 2012.

https://doi.org/10.5194/essd-2019-79
Preprint. Discussion started: 1 July 2019

Open Access Earth System Science Data Discussions

Variable description	Units	Resolution (lon×lat), time	Notes	Variable name(s)	PMIP3 variable name(s)
Specific humidity	kg kg^{-1}	192×94, 1460	Re-referenced to 10 m	huss_10m	huss
Downwelling longwave radiation	W m^{-2}	192×94, 365		rlds	rlds
Downwelling shortwave radiation	W m^{-2}	192×94, 365		rsds	rsds
Precipitation	mm day^{-1}	192×94, 12		pr	pr
Wind (u and v components)	m s^{-1}	192×94, 1460		uas and vas	uas and vas
Temperature	K	192×94, 1460	Re-referenced to 10 m	tas (re-referenced) tas_10m (re-referenced and topography corrected) tas_diff (= tas - tas_10m = temperature effect)	tas
Sea surface salinity	psu	360×180, 12	CNRM-CM5 and MIROC-ESM only	sos	sos

Table 1: Summary of the data showing variable description, units, format (lon×lat, time), Notes, netCDF variable name(s) and the original PMIP3 variable name(s). The wind component variables are provided in separate files (Morée and Schwinger, 2019).

https://doi.org/10.5194/essd-2019-79
Preprint. Discussion started: 1 July 2019

Model name	Modelling group	Reference
CNRM-CM5	CNRM-CERFACS (France)	Voldoire et al. (2013)
IPSL-CM5A-LR	IPSL (Institut Pierre Simon Laplace, France)	Dufresne et al. (2013)
MIROC-ESM	MIROC (JAMSTEC and NIES, Japan)	Sueyoshi et al. (2013)
MRI-CGCM3	MRI (Meteorological Research Institute, Japan)	Yukimoto et al. (2012)

Table 2: PMIP3 models used in this study

https://doi.org/10.5194/essd-2019-79
Preprint. Discussion started: 1 July 2019

#	CDO or NCO command
1	cdo remapbil,t62grid
2	ncea
3	ncdiff
4	ncap2
5	cdo inttime
6	cdo setmisstodis
7	cdo smooth9

Table 3: Package commands applied in this study. Detailed information on these commands can be found in the respective NCO and CDO documentation online. All operations were performed with either CDO version 1.7.0 (Schulzweida, 2019) or NCO version 4.6.9.

https://doi.org/10.5194/essd-2019-79
Preprint. Discussion started: 1 July 2019

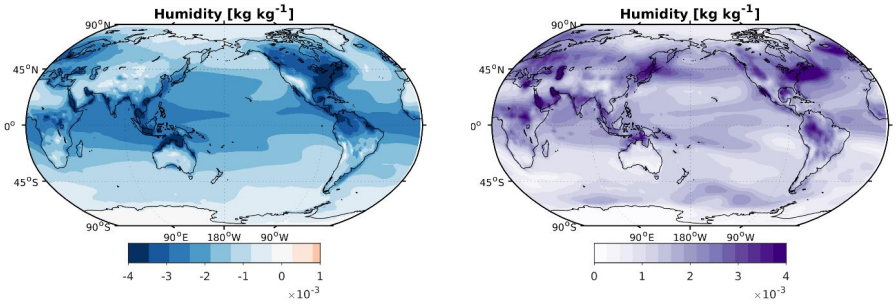

Figure 1: Annual mean 10-meter height specific humidity LGM-PI anomaly (left) and model spread (right) in kg kg^{-1}.

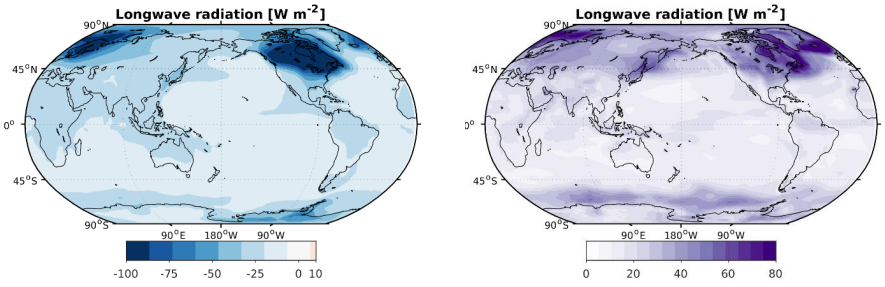

Figure 2: Annual mean downwelling longwave radiation LGM-PI anomaly (left) and model spread (right) in W m^{-2}.

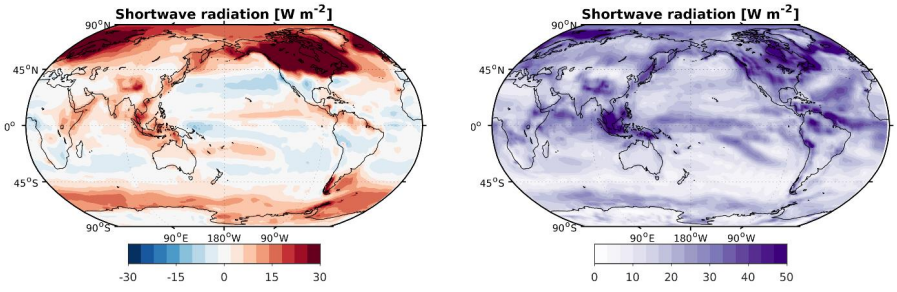

Figure 3: Annual mean downwelling shortwave radiation LGM-PI anomaly (left) and model spread (right) in W m^{-2}.

https://doi.org/10.5194/essd-2019-79
Preprint. Discussion started: 1 July 2019

Open Access Earth System Science Data Discussions

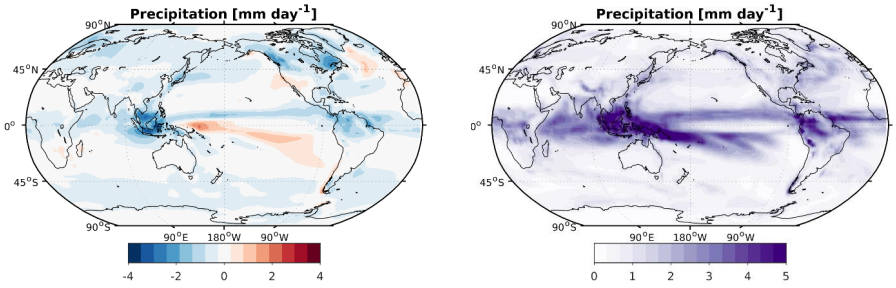

Figure 4: Annual mean precipitation LGM-PI anomaly (left) and model spread (right) in mm day^{-1}.

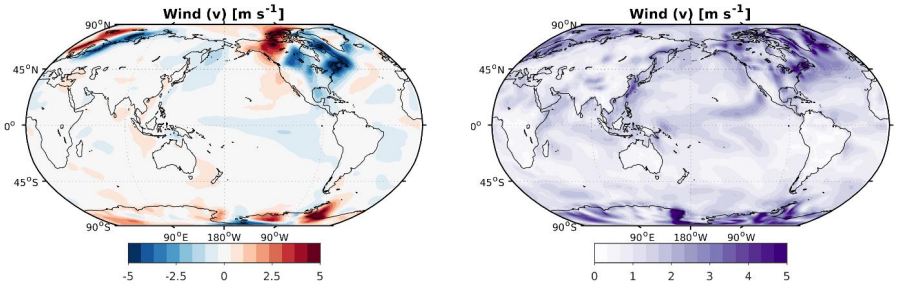

Figure 5: Annual mean meridional wind velocity LGM-PI anomaly (left) and model spread (right) in m s^{-1}.

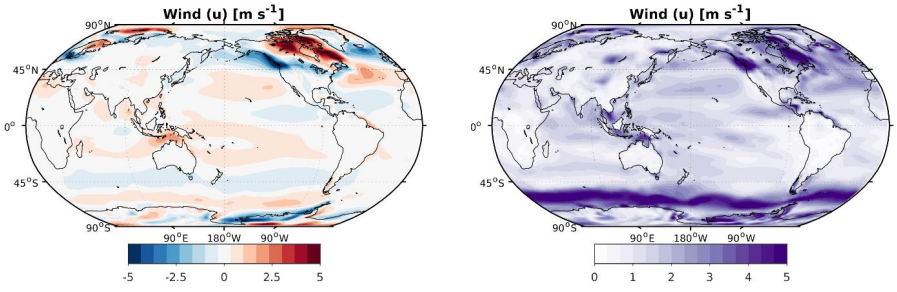

5

Figure 6: Annual mean zonal wind velocity LGM-PI anomaly (left) and model spread (right) in m s^{-1}.

https://doi.org/10.5194/essd-2019-79
Preprint. Discussion started: 1 July 2019

Open Access Earth System Science Data Discussions

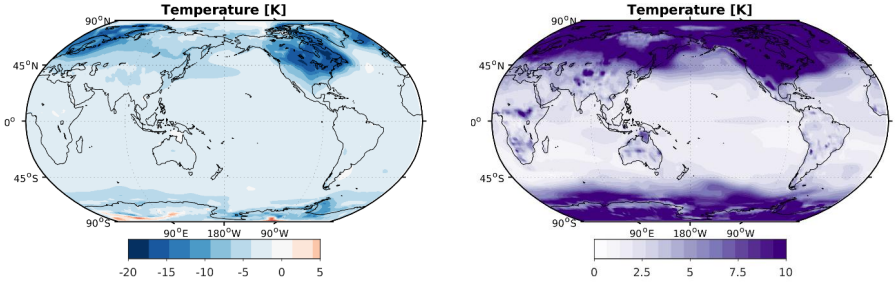

Figure 7: Annual mean topography-corrected 10-meter height temperature LGM-PI anomaly (left) and model spread (right) in K.

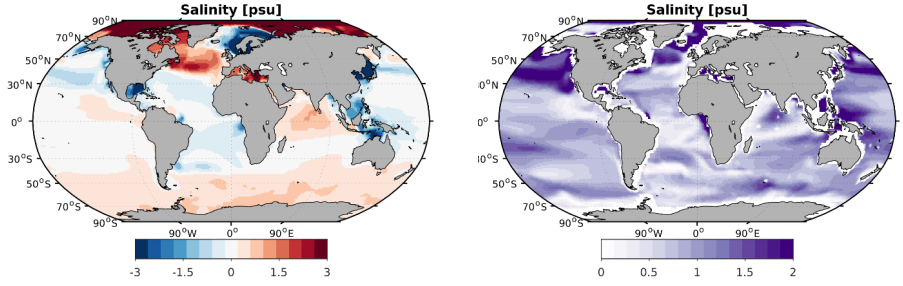

Figure 8: Annual mean sea surface salinity LGM-PI anomaly (left) and model spread (right) in psu.